

Sphingolipid profile alters in retinal dystrophic P23H-1 rats and systemic FTY720 can delay retinal degeneration[§]

Megan Stiles,^{*,†} Hui Qi,^{*,†} Eleanor Sun,^{*,†} Jeremy Tan,^{*,†} Hunter Porter,^{*,†} Jeremy Allegood,[§] Charles E. Chalfant,^{§,***,††,§§} Douglas Yasumura,^{***} Michael T. Matthes,^{***} Matthew M. LaVail,^{***} and Nawajes A. Mandal^{1,*,†,††,§§§,****}

Department of Ophthalmology,* Department of Physiology,^{†††} Department of Cell Biology,^{§§§} and Oklahoma Center for Neuroscience,^{****} University of Oklahoma Health Sciences Center, Oklahoma City, OK 73104; Dean McGee Eye Institute,[†] Oklahoma City, OK 73104; Research and Development,^{**} Hunter Holmes McGuire Veterans Administration Medical Center, Richmond, VA 23249; Department of Biochemistry and Molecular Biology,[§] Virginia Commonwealth University School of Medicine, Virginia Commonwealth University Massey Cancer Center,^{††} Virginia Commonwealth University Institute of Molecular Medicine and the Virginia Commonwealth University Johnson Center,^{§§} Virginia Commonwealth University, Richmond, VA 23298; and Beckman Vision Center,^{***} University of California, San Francisco School of Medicine, San Francisco, CA 94143

Abstract Retinal degeneration (RD) affects millions of people and is a major cause of ocular impairment and blindness. With a wide range of mutations and conditions leading to degeneration, targeting downstream processes is necessary for developing effective treatments. Ceramide and sphingosine-1-phosphate, a pair of bioactive sphingolipids, are involved in apoptosis and its prevention, respectively. Apoptotic cell death is a potential driver of RD, and in order to understand the mechanism of degeneration and potential treatments, we studied rhodopsin mutant RD model, P23H-1 rats. Investigating this genetic model of human RD allows us to investigate the association of sphingolipid metabolites with the degeneration of the retina in P23H-1 rats and the effects of a specific modulator of sphingolipid metabolism, FTY720. We found that P23H-1 rat retinas had altered sphingolipid profiles that, when treated with FTY720, were rebalanced closer to normal levels. FTY720-treated rats also showed protection from RD compared with their vehicle-treated littermates.^{¶¶} Based on these data, we conclude that sphingolipid dysregulation plays a secondary role in retinal cell death, which may be common to many forms of RDs, and that the U.S. Food and Drug Administration-approved

drug FTY720 or related compounds that modulate sphingolipid metabolism could potentially delay the cell death.—Stiles, M., H. Qi, E. Sun, J. Tan, H. Porter, J. Allegood, C. E. Chalfant, D. Yasumura, M. T. Matthes, M. M. LaVail, and N. A. Mandal. **Sphingolipid profile alters in retinal dystrophic P23H-1 rats and systemic FTY720 can delay retinal degeneration.** *J. Lipid Res.* 2016. 57: 818–831.

Supplementary key words retina • P23H line 1 rats • photoreceptors • apoptosis • ceramide • hexosyl-ceramide • sphingomyelin • FTY720 • fingolimod • sphingomyelinase

Retinal degenerations (RDs), a heterogeneous group of diseases, are characterized by photoreceptor cell death by apoptosis. While the mechanism of disease development and many causative mutations have been identified for RDs, very few new therapies have been developed due to the genetic diversity of this group of diseases. More than 200 gene mutations are currently known for hereditary RDs (<https://sph.uth.edu/Retnet/sum-dis.htm>). Research

This work was supported by National Center for Research Resources grant RR17703, National Eye Institute grants EY022071, EY021725, EY025256, EY001919, EY006842, EY002162, Foundation Fighting Blindness, and Research to Prevent Blindness Inc. USA. Tuan-Phat Huynh, Mark Dittmar, Louisa J. Williams, and Linda S. Boone (from the Department of Ophthalmology, University of Oklahoma Health Sciences Center, Oklahoma City, OK) are gratefully acknowledged by the authors for the technical support they provided. This work was also supported by research grants from the Veterans Administration (VA Merit Review 1 BX001792 [C.E.C.] and an RCS Award 13F-RCS-002 [C.E.C.]) and from the National Institutes of Health (HL125353 [C.E.C.]). Services [Virginia Commonwealth University (VCU) Lipidomics/Metabolomics Core] and products in support of the study were generated, in part, by the VCU Massey Cancer Center with funding from National Institutes of Health Grant P30 CA016059. The content is solely the responsibility of the authors and does not necessarily represent the official views of the National Institutes of Health, the Department of Veterans Affairs, or the U.S. government.

Manuscript received 11 September 2015 and in revised form 6 February 2016.

Published, JLR Papers in Press, March 5, 2016

DOI 10.1194/jlr.M063719

Abbreviations: Asah, acyl-sphingosine amido-hydrolase; aSMase, acidic sphingomyelinase; C1P, ceramide 1-phosphate; Cer, ceramide; CerS, ceramide synthase; ERG, electroretinography; Gcs, glucosylceramide synthase; Gfap, glial fibrillary acidic protein; GS, glutamine synthetase; H and E, hematoxylin and eosin; Hex-Cer, hexosyl-ceramide; IHC, immunohistochemical; IR, ionizing radiation; nSMase, neutral sphingomyelinase; ONL, outer nuclear layer; P, postnatal day; P23H-1, P23H line 1; qRT-PCR, quantitative RT-PCR; RD, retinal degeneration; RP, retinitis pigmentosa; RPE, retinal pigment epithelia; S1P, sphingosine 1-phosphate; SD, Sprague Dawley; Smpd, sphingomyelin phosphodiesterase; Sms, sphingomyelin synthase; Sph, sphingosine; Sphk, sphingosine kinase; SPT, serine palmitoyl transferase.

¹To whom correspondence should be addressed.

e-mail: mmandal@ouhsc.edu

[§]The online version of this article (available at <http://www.jlr.org>) contains a supplement.

in recent time suggests that inflammation precedes the death of photoreceptor and retinal pigment epithelial (RPE) cells in many forms of human RDs including age-related macular degeneration (AMD), diabetic retinopathy, and retinitis pigmentosa (RP) (1–7). Through our previous studies, we have found that the signaling sphingolipid ceramide (Cer) acts as a modulator in RD (8). We found that Cer levels increase during RD in a rodent model of light-stress-induced RD and that systemic administration of a pharmacological compound, FTY720, which can inhibit Cer synthesis (9, 10), blocks Cer increase, and protects the retina from degeneration (8).

FTY720 is an analog of sphingosine (Sph) and can be phosphorylated to FTY720-P *in vivo* by sphingosine kinase (SPHK) 2 to mimic the action of sphingosine 1-phosphate (S1P) (11–14). The signaling sphingolipids such as Cer, ceramide-1-phosphate (C1P), Sph, and S1P act as important mediators of cell function and are fundamentally involved in many cellular processes (15–19). Cer induces proapoptotic signaling, whereas S1P has an opposing intracellular role (i.e., protection against cell death) (16, 17, 19). Based on our research findings thus far, we propose that a delicate balance between Cer and S1P is important in maintaining normal photoreceptor structure and function.

In our search for a *de novo* Cer biosynthetic inhibitor that is not neurotoxic and could be delivered systemically, we encountered the compound FTY720. FTY720 is derived from the compound myriocin but has a much lower *in vivo* toxicity rate. After three phases of human clinical trials, FTY720 (Gilenya, Novartis) has been approved for human relapsing multiple sclerosis, mainly for its immunosuppressive property (11, 20–22). However, FTY720 is also known to inhibit ceramide synthase (CerS) and block *de novo* Cer production (9, 10, 23). In a previous publication, we used our light-stress albino rat model and demonstrated that systemic (intraperitoneal) administration of FTY720 could block the light-induced increase in Cer levels in the retinas and significantly prevented light-induced damage of retinal structure and function (8).

To test further the changes in the sphingolipid profile in other genetic models of RDs, we used P23H line 1 (P23H-1) rats, a popular model of human RD, developed by Matthew M. LaVail, in which photoreceptor degeneration starts at the beginning of light responsiveness at approximately postnatal day (P) 15 and 50% of photoreceptors die by P45 (24, 25). In the P23H-1 model, we found an increase in major sphingolipid species including bioactive Cer, hexosylceramide (Hex-Cer), and S1P species that are associated with cellular signaling. We further demonstrate here that sphingolipid changes can be reverted or modulated to some extent by systemic administration of FTY720, which can delay the progression of RD.

EXPERIMENTAL PROCEDURES

Animal care

All procedures were performed according to the Association for Research in Vision and Ophthalmology Statement for the

Use of Animals in Ophthalmic and Vision Research and the University of Oklahoma Health Sciences Center Guidelines for Animals in Research. All protocols were reviewed and approved by the Institutional Animal Care and Use Committee of the University of Oklahoma Health Sciences Center. Albino Sprague-Dawley (SD) rats and P23H-1 rats were born and raised in the Dean A. McGee Eye Institute vivarium and maintained from birth under dim cyclic light (5 lux, 12 h on/off, 7 AM to 7 PM central time).

Systemic dosing of FTY720 in juvenile P23H-1 rats

P23H-1 rats were dosed systemically (intraperitoneally) twice weekly with 2.5 mg/kg FTY720 from P10 to P21, after which the rats were weaned from their mother and the twice weekly dosing was raised to 5 mg/kg until P45. At P35, the rats underwent electroretinography (ERG) functional analysis. Rats were euthanized by carbon dioxide asphyxiation for tissue analysis at either P22 or P45 in order to compare age points. Another group of rats were euthanized at P35 and their eyes were either harvested for histological structural analysis as well as immunohistochemistry staining or retinas were snap frozen in liquid nitrogen for RT-PCR and chemical analysis of sphingolipids. Age-matched SD rats were used as a model control.

ERG

Flash ERGs were recorded with the Diagnosys Espion E2 ERG system (Diagnosys LLC, Lowell, MA). Rats were maintained in total darkness overnight and prepared for ERG recording under dim red light. They were anesthetized with ketamine (100 mg/kg body weight) and xylazine (5 mg/kg body weight) intraperitoneally. One drop of 10% (v/v) phenylephrine was applied to the cornea to dilate the pupil, and one drop of 0.5% (v/v) proparacaine HCl was applied for local anesthesia. Rats were kept on a heating pad at 37°C during recordings. A gold electrode was placed on the cornea, a reference electrode was positioned in the mouth, a ground electrode was placed in the tail, and rats were placed inside a Ganzfeld illuminating sphere. Responses were differentially amplified, averaged, and stored. For the assessment of rod photoreceptor function (scotopic ERG), five strobe flash stimuli were presented at flash intensities at -2.3 , -1.3 , 0.7 , 2.7 , and $3.3 \log \text{cd}\cdot\text{s}/\text{m}^2$. The amplitude of the a-wave was measured from the prestimulus base line to the a-wave trough. The amplitude of the b-wave was measured from the trough of the a-wave to the peak of the b-wave. For the evaluation of cone function (photopic ERG), a strobe flash stimulus ($3.3 \log \text{cd}\cdot\text{s}/\text{m}^2$) was presented to dilated, light-adapted (5 min at $1.7 \log \text{cd}\cdot\text{s}/\text{m}^2$) rats. Photopic, blue and green cone, and 3, 10, 20, and 30 Hz flickers were used for cone functional analysis. The amplitude of the cone b-wave was measured from the trough of the a-wave to the peak of the b-wave.

Histology

After euthanizing by carbon dioxide asphyxiation at specific ages, rat eyes were enucleated, immediately after death, placed in fixative (Prefer; Anatech LTD, Battle Creek, MI), and embedded in paraffin for light microscope evaluation of retinal structure. Sections of 5 μm were cut along the vertical meridian through the optic nerve and stained with hematoxylin and eosin (H and E). The thickness of the outer nuclear layer (ONL) was measured at 0.5 mm distances from the optic nerve to the inferior and superior ora serrata and plotted as a spider diagram. Unstained slides were also obtained in order to perform immunohistochemical (IHC) analysis.

Sphingolipid analysis

Internal standards were purchased from Avanti Polar Lipids (Alabaster, AL). Internal standards were added to samples in 20 μl

ethanol-methanol-water (7:2:1) as a cocktail of 500 pmol each. Standards for sphingoid bases and sphingoid base 1-phosphates were 17-carbon chain length analogs: C17-sph, C17-sphinganine, C17-S1P, and C17-sphinganine 1-phosphate. Standards for *N*-acyl sphingolipids were C12-fatty acid analogs: C12-Cer, C12-C1P, C12-SM, and C12-glucosylceramide. The MS-grade solvents (chloroform and methanol, as well as formic acid) were obtained from VWR (West Chester, PA).

For LC/MS/MS analyses, a Shimadzu LC-20 AD binary pump system coupled to a SIL-20AC autoinjector and DGU20A3 degasser coupled to an ABI 4000 quadrupole/linear ion trap (QTrap) (Applied Biosystems, Foster City, CA) operating in a triple quadrupole mode was used. Q1 and Q3 was set to pass molecularly distinctive precursor and product ions (or a scan across multiple *m/z* in Q1 or Q3), using N2 to collisionally induce dissociations in Q2 (which was offset from Q1 by 30–120 eV); the ion source temperature set to 500°C.

Extraction and analysis of sphingolipids. Samples were collected into 13 × 100 mm borosilicate tubes with a Teflon-lined cap (VWR). Then 1 ml of CH₃OH and 0.5 ml of CHCl₃ were added along with the internal standard cocktail (500 pmol of each species dissolved in a final total volume of 20 μl of ethanol-methanol-water, 7:2:1). The contents were dispersed using an ultrasonicator at room temperature for 30 s. This single phase mixture was incubated at 48°C overnight. After cooling, 75 μl of 1 M KOH in CH₃OH was added and, after a brief sonication, was incubated in a shaking water bath for 2 h at 37°C to cleave potentially interfering glycerolipids. The extract was brought to neutral pH with 6 μl of glacial acetic acid, then the extract was centrifuged using a table-top centrifuge, and the supernatant was removed by a Pasteur pipette and transferred to a new tube. The extract was reduced to dryness using a Speed Vac. The dried residue was reconstituted in 0.5 ml of the starting mobile phase solvent for LC/MS/MS analysis, sonicated for 15 s, then centrifuged for 5 min in a table-top centrifuge before transfer of the clear supernatant to the autoinjector vial for analysis.

Sphingoid bases, sphingoid base 1-phosphates, and complex sphingolipids were separated by reverse phase LC using a Supelco 2.1 (inner diameter) × 50 mm Ascentis Express C18 column (Sigma, St. Louis, MO) and a binary solvent system at a flow rate of 0.5 ml/min with a column oven set to 35°C. Prior to injection of the sample, the column was equilibrated for 0.5 min with a solvent mixture of 95% mobile phase A1 (CH₃OH/water/HCOOH, 58:41:1, v/v/v; with 5 mM ammonium formate) and 5% mobile phase B1 (CH₃OH/HCOOH, 99:1, v/v; with 5 mM ammonium formate), and after sample injection (typically 40 μl), the A1/B1 ratio was maintained at 95:5 for 2.25 min, followed by a linear gradient to 100% B1 over 1.5 min, which was held at 100% B1 for 5.5 min, followed by a 0.5 min gradient return to 95:5 A1/B1. The column was reequilibrated with 95:5 A1/B1 for 0.5 min before the next run.

The species of Cer, Hex-Cer, SM, sphingoid lipids such as Sph, dihydro (Dh)-Sph, S1P, and Dh-S1P were identified based on their retention time and *m/z* ratio and quantified as described in previous publications (26, 27).

RT-PCR

RNA was isolated from collected rat retinal tissue using RNeasy Plus Mini kit (Invitrogen). Following the manufacturer's protocol: 1.0 μg of total RNA from each tissue was converted to cDNA using SuperScript III First-Strand Synthesis supermix (Invitrogen) for quantitative RT-PCR (qRT-PCR). Primers for qRT-PCR were designed in such a way that they spanned at least one intron, which eliminated the chance of amplification from residual genomic

DNA contamination. Sequences of the primers may be obtained from the corresponding author upon request. Quantitative PCR and melt-curve analyses were performed using iTaq Universal SYBR Green Supermix (Bio-Rad, Hercules, CA) and an iCycler machine. Relative quantities of expression of the genes of interest in different samples were calculated by the comparative Ct (threshold cycle) value method (8, 28–30).

SMase assay

Acidic and neutral sphingomyelinase (aSMase and nSMase, respectively) activity was indirectly measured in the retinal protein using the Amplex Red Sphingomyelinase Assay Kit (Invitrogen). Retinas were homogenized in T-PER buffer (Pierce, Rockford, IL) with a protease inhibitor cocktail and centrifuged at 10,000 rpm for 10 min at 4°C. The protein concentration in the supernatant fraction was measured with the BCA protein assay (Pierce), and the activity of aSMase and nSMase was determined by modulating the pH of the reaction buffer and following the manufacturer's protocol.

Immunohistochemistry

Immunolabeling on paraffin sections was performed as follows: sections were deparaffinized, rinsed for 30 min with PBS containing 0.1% Triton X-100. A blocking step was performed using 10% normal horse serum. Sections were then incubated overnight in the primary antibody; anti-mouse rhodopsin (Abcam, Cambridge, MA), rhodamine peanut agglutinin (Vector Laboratories, Burlingame, CA), anti-mouse glutamine synthetase (GS) (Millipore, Billerica, MA), anti-goat glial fibrillary acidic protein (GFAP) (Sigma), anti-rabbit SPHK2 (AbNOVA, Walnut, CA), anti-rabbit acyl-sphingosine amido-hydrolase (ASAH) 1 (Sigma) diluted 1:200 in PBS. After rinsing, sections were washed three times for 10 min with PBS containing 0.5% TritonX-100. Sections were rinsed and cover-slipped with ProLong Gold antifade reagent with 4',6-diamidino-2-phenylindole (Invitrogen, Carlsbad, CA).

Statistical analyses

Statistical analyses were performed using GraphPad Prism 5.0 software (GraphPad Software Inc., La Jolla, CA). The quantitative data are expressed as mean ± SE for each group. One-way or two-way ANOVA and Student's and paired *t*-tests were performed to assess differences between means.

RESULTS

Systemic FTY720 reduces photoreceptor degeneration in P23H-1 rats

Photoreceptors of P23H-1 rats degenerate at a fast rate starting from P15, when their eyes are first opened and exposed to light. Beginning at P10, P23H-1 rat pups were dosed systemically with 2.5 mg/kg of FTY720 twice weekly until they reached P21, after which the amount of FTY720 delivered was increased to 5 mg/kg. At P35 the rats underwent ERG functional analysis using age-matched SD controls. In FTY720-treated P23H-1 rats, we observed a functional increase in ERG response in both the a- and b-wave amplitudes compared with vehicle-treated littermates (Fig. 1A). Cone function (photopic) analysis also resulted in an increase in b-wave amplitude at most of the flashes tested, with significant preservation in blue light flash, 10 Hz, and 20 Hz flickers (Fig. 1B; *P* < 0.05). FTY720 treatment in

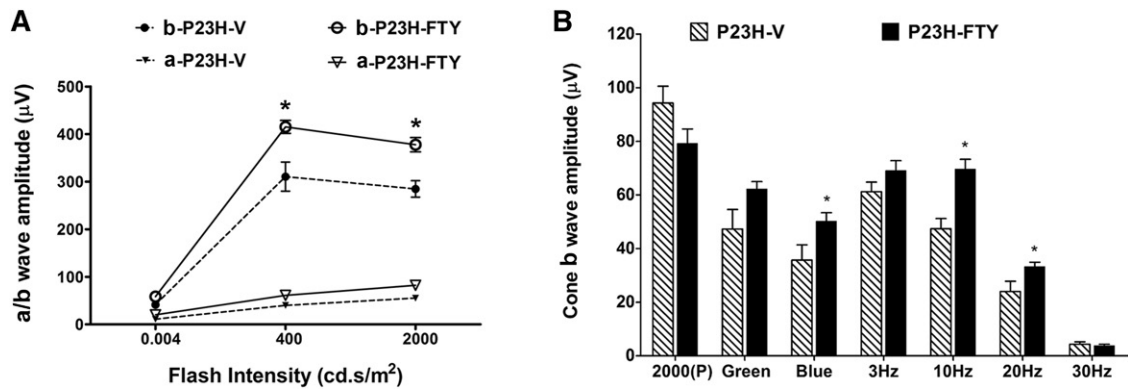


Fig. 1. Electrophoretographic measurement of retinal function in FTY720-treated P23H-1 rats. P23H-1 rat pups were dosed systemically with 2 FTY720 twice weekly started at P10. At P35 ERG responses for scotopic function were recorded for three flash stimuli at intensities of 0.004, 400, and 2,000 $\text{cd}\cdot\text{s}/\text{m}^2$ were recorded to assess retinal function. The a-wave represents the responses obtained directly from photoreceptor cells, while the b-wave represents the response obtained by both the photoreceptors and primarily downstream secondary neurons. A: Scotopic response for both a- and b-waves; FTY720-treated P23H-1 rats showed higher b-wave responses. B: Photopic response of cone b-wave. * $P < 0.05$; Student's t -test ($n = 8-10$). P23H-FTY, FTY720-treated P23H-1 rhodopsin mutant rats; P23H-V, vehicle-treated P23H-1 rhodopsin mutant rats.

SD rats did not cause any functional changes in retinal light responses (data not shown).

Histological analysis of ONL thickness at P45 revealed differences in the retinal preservation of photoreceptor cells in P23H-1 rats treated with FTY720 (Fig. 2). P23H-1 rats had vastly decreased ONL thickness compared with SD controls (Fig. 2A). FTY720 had limited effects on ONL thickness in SD rats, but P23H-1 rats treated with FTY720 displayed significantly increased ONL thickness compared with vehicle controls (Fig. 2A; $P < 0.01$). When measuring the ONL thickness in the central retina (closest five points to the optic nerve of either the inferior or superior hemispheres), we observed a significant increase in both inferior and superior ONL thickness in P23H-1 rats that had been treated with FTY720 (Fig. 2B; $P < 0.01$; $n = 8-10$). Representative histological images of the superior central retina of both SD and P23H-1 rats show the same (Fig. 2C-F).

Spingolipid profile alters in P23H-1 rat retina

There is no previous study on the spingolipid composition of degenerating P23H-1 rat retina. We studied the retinal composition of major spingolipid classes in P23H-1 rats at two age points, P22 and P45. At P22, P23H-1 rats degenerate $\sim 20\%$ of total photoreceptors, and by P45, the loss is $>50\%$ of their photoreceptors (24, 25). P23H-1 rats were treated with FTY720 with littermates used as vehicle controls. In a parallel experiment, SD rats were also treated with either FTY720 or vehicle and harvested at similar time points serving as wild-type controls. Among the major classes of spingolipids, we found total Cer increases significantly in P23H-1 retina at P22, but at P45, however, no change was seen (Fig. 3A; $\# P < 0.01$). We also found systemic long-term FTY720 did not affect the Cer levels in SD retina (Fig. 3A). Cer is the key metabolite for the all classes of higher order and complex spingolipids, and its level is very tightly regulated by a group of anabolic and catabolic enzymes. A significant increase in Cer

anabolic products Hex-Cer and SM was found in P23H-1 retina at P22 (Fig. 3B, C; $P < 0.01$), as well as a significant increase of Cer catabolic or downstream product SIP (Fig. 3D; $P < 0.01$). Interestingly, the levels of all three later classes of lipids were downregulated by the treatment of FTY720 in P23H-1 retina (Fig. 3B-D; * $P < 0.01$). We therefore conclude that P23H-1 retina accumulates Cer and its metabolic products significantly at early stages before major degeneration occurs (P22), and systemic treatment of FTY720 could downregulate the metabolic products of Cer. In P45 SD rats, long-term treatment of FTY720 seems to have reduced the level of total Hex-Cer, SM, and SIP in (Fig. 3B-D; * $P < 0.01$). In P45 P23H-1 retina, which has lost $>50\%$ of photoreceptor cells, there was no difference found in the levels of Cer and Hex-Cer, but SM, the major structural species, was reduced significantly compared with SD control retina (Fig. 3A-C; $\# P < 0.01$), which indicates a higher ratio of Cer and Hex-Cer in P23H-1 retina at P45. However, at this stage of RD (P45), no effect of FTY720 was detected on their levels (Fig. 3B-D).

We further investigated if the relative composition of the major spingolipid groups altered in the P23H-1 retina and how that was modulated when the rats were treated with FTY720. At P22, there was no change in the relative levels of Cer in P23H-1 retina compared with SD control (59% in each), but there was an increase in Hex-Cer (3% vs. 5%) and a decrease in SM levels (38% vs. 36%) (Fig. 4). When these rats were treated systemically with FTY720, the relative composition did not change much in SD rats, but in P23H-1 rats, the Hex-Cer composition reduced to 4% (Fig. 4). Interestingly, the relative composition of major spingolipid groups was vastly different in P45 retina from P22 retina. In vehicle-treated SD rats, the ratio of Cer:Hex-Cer:SM was 20:9:71 compared with P22 where the ratio was 59:3:38 (Fig. 4), which did not change when treated with FTY720. The ratio in P23H-1 retina at P45, however, was 24:16:60, reflecting relatively much higher levels of

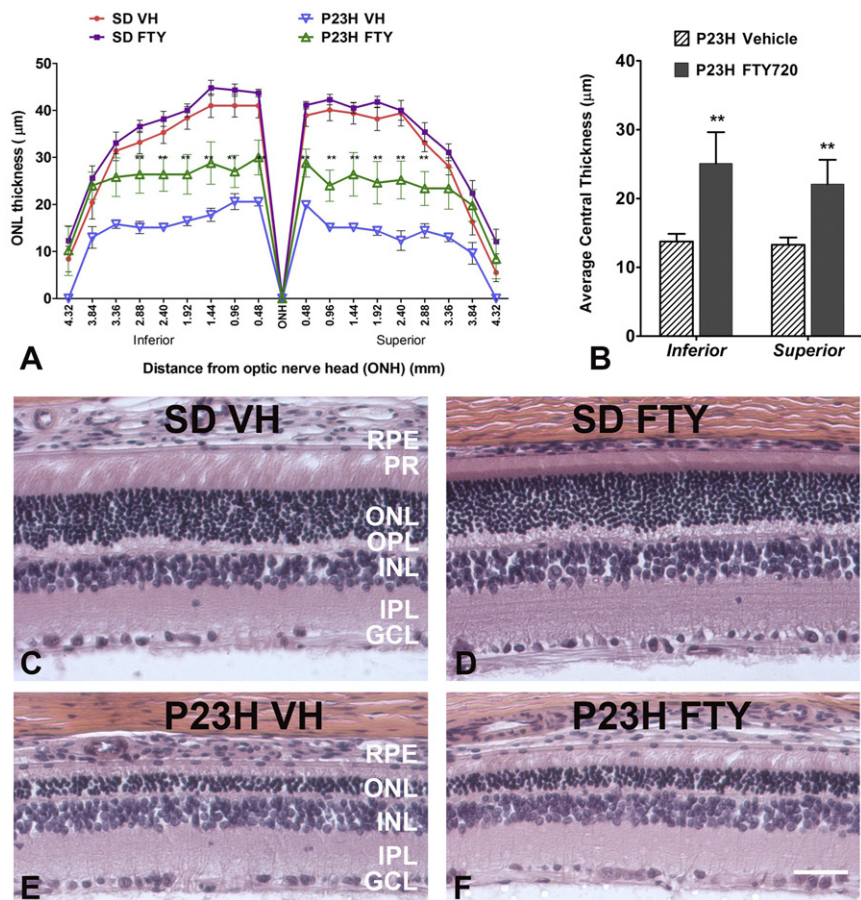


Fig. 2. Retinal histology analysis and protection of photoreceptor cell death in FTY720-treated P23H-1 rats. A: Spider plot generated from quantitative morphometric measurement of average ONL thickness in each strain/treatment combination (\pm SE) using H and E-stained slides from P45 rat retinas. B: Graph of inferior and superior ONL thickness averages (\pm SE). Inferior data are the average of the five points closest to the ONH on the inferior side; superior is measured in the same manner on the superior side. Representative images of H and E-stained retinas: vehicle-treated SD rat control (C), FTY720-treated SD rat control (D), vehicle-treated P23H-1 rat (E), and FTY720-treated P23H-1 rat (F). FTY, FTY720; GCL, ganglion cell layer; INL, inner nuclear layer; IPL, inner plexiform layer; ONH, optic nerve head; OPL, outer plexiform layer; P23H, P23H rhodopsin mutant strain 1; PR, photoreceptor; VH, vehicle. ** $P < 0.01$, compared with vehicle treatment in the same strain; Student's *t*-test ($n = 8-10$).

Cers and Hex-Cers compared with SD retina (40% vs. 29%), which was not decreased by the treatment of FTY720 (41%) (Fig. 4).

In summary, all major species of sphingolipids increased in P23H-1 retina at an early stage of degeneration at which $\sim 20\%$ photoreceptor cells are degenerated. Considering photoreceptor cells are the major contributor of retinal cell populations, the increase in sphingolipid metabolites resulted from metabolic changes rather than changes in cell population. It is also clear from the SD rat data that long-term systemic FTY720 has an effect in reducing the metabolic products of Cer, rather than the Cer level itself, which was also observed for P23H-1 retina at P22. At P45, with the majority of photoreceptors degenerated in P23H-1 retina, no effect of FTY720 was found. However, the relative levels of Cer and Hex-Cer are much higher in P23H-1 retina at P45 compared with SD controls, further indicating a metabolic change associated with the degenerating photoreceptors.

Assessment of SMase activity

FTY720 is known to inhibit de novo Cer biosynthesis. As we did not see a reduction of Cer in FTY720-treated P23H-1 retina, we assessed the activity of the neutral and acidic SMases, one or both of which may be activated and maintaining the higher Cer levels in P23H-1 retinas. We observed at P22 no significant difference between rat strains in aSMase, but a significant increase in nSMase in the P23H-1 retinas (Fig. 5; $P < 0.05$). FTY720 had no significant effect on either SMase in control SD rats but significantly increased aSMase activity and decreased nSMase activity in P23H-1 rats (Fig. 5; $P < 0.05$). Thus, it is apparent that increases in nSMase activity contributed to the levels of increased Cer in P23H-1 retina; FTY720 could reduce this activity to some extent (albeit not to the normal level), but at the same time increased aSMase activity, which maintained the higher levels of Cer in P23H-1 retina. It should be noted that FTY720 could delay the degeneration of photoreceptors in P23H-1 retina but could not

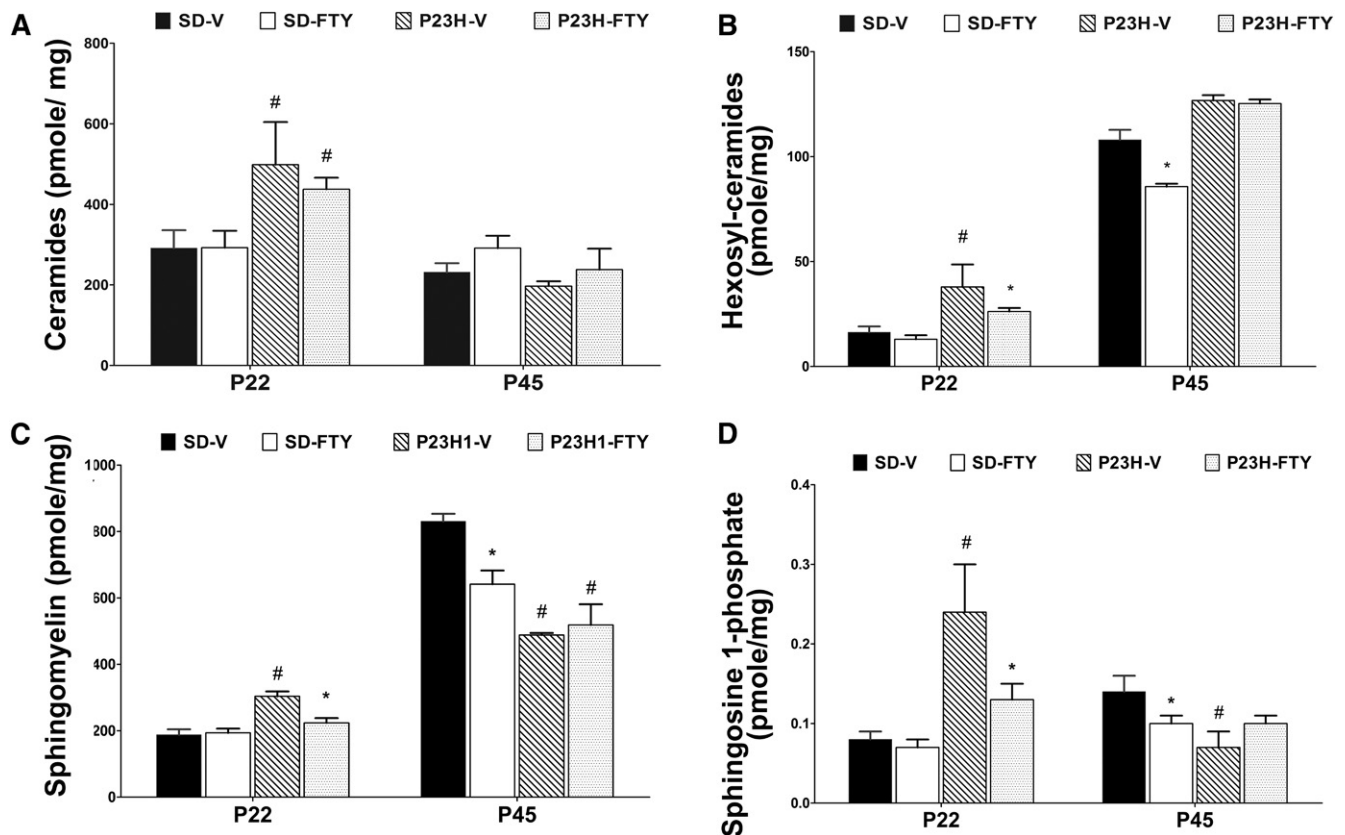


Fig. 3. Analysis of retinal sphingolipids in P23H-1 and SD rat retina at age P22 and P45. Retinas were harvested from rats at P22 and P45, processed to collect sphingolipids, and analyzed using LC/MS/MS. Data represented as total pmol/mg of each lipid category in each strain/treatment combination. The “#” indicates significant change in P23H-1 retina from SD retina, and “*” indicates significant change after FTY720 treatment ($P < 0.01$, $n = 4$). A: Analysis of retinal Cers. P23H-1-FTY was significantly different from SD-FTY at P22. B: Analysis of retinal Hex-Cers. P23H-1-V was significantly different from SD-V and P23H-1-FTY at P22. C: Analysis of retinal SMs. P23H-1-V was significantly different from SD-V and P23H-1-FTY at P22; P23H-1-V and P23H-1-FTY were significantly different from their SD controls, and SD-FTY was significantly different from SD-V at P45. D: Analysis of retinal S1P. P23H-1-V had significantly greater S1P compared with SD-V, while P23H-1-FTY had significantly lower S1P compared with P23H-1-V at P22; P23H-1-V and SD-FTY had significantly reduced S1P compared with SD-V at P45. SD-FTY, FTY720-treated Sprague-Dawley rats; SD-V, vehicle-treated Sprague-Dawley rats.

prevent it beyond a certain point, which could be due to the generation of Cer from other pathways that contributed to the cell death.

Analysis of individual sphingolipid species

There are many species of Cer and its metabolites in a cell (31). Accumulating evidence suggests varied roles of different species of Cer and its metabolites. In order to determine whether any particular species, metabolite, or a group of species play a major role in the photoreceptor degeneration process, we evaluated the absolute and relative composition of major species of Cer, Hex-Cer, and SM.

Composition of Cer species. As seen for the total amount of Cer, the levels of major species of Cer in P23H-1 P22 retina were also analyzed (Table 1). FTY720 treatment appears to have reduced the levels of each species of Cer: saturated or monounsaturated, short-chain or long-chain. However, due to higher variability and lower sample numbers, the data did not reach a statistically significant level (Table 1; $P < 0.01$, $n = 4$). At P45, we did not see a difference

in absolute composition of various species of Cer in P23H-1 retina compared with SD retina (Table 1).

We further analyzed the changes in relative composition of the major Cer species in P23H-1 retina. Relative composition of long-chain Cers (22:0; 24:1; 24:0) increased from 13 mol % (4% + 6% + 3%) to 19 mol % (5% + 9% + 5%) in P23H-1 retina (supplementary Figure 1A vs. E), out of which 22:0 and 24:0 was reduced by 1% each after FTY720 treatment (supplementary Figure 1E vs. F).

We found a similar trend in the relative compositions of various Cer species in P45 P23H-1 retina. The proportion of shorter-chain Cers (C16:0 and C18:0) decreased (75% to 68%) and the proportion of long-chain Cers (C20:0–C24:0) increased (25% to 32%) (supplementary Figure 1C vs. G). Long-term FTY720 treatment did not affect the relative composition of Cers in the SD retinas (supplementary Figure 1C vs. D); however, it modified the ratio in P23H-1 retina (68% to 72% short-chain Cers and 32% to 28% long-chain Cers) (supplementary Figure 1G vs. H).

Composition of Hex-Cer species. As seen for the total amount of Hex-Cer the levels of all the major species of

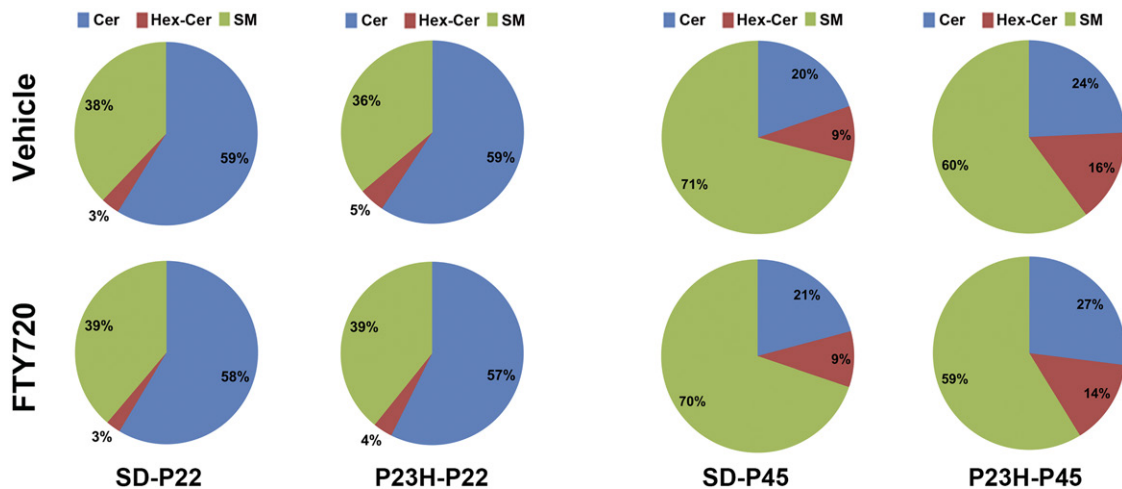


Fig. 4. Compositional analysis of the major classes of sphingolipids in P23H-1 and SD rat retina at age P22 and P45. Retinas were harvested, processed to collect sphingolipids, and analyzed using LC/MS/MS. Pie charts developed from compositional analysis of the total amount of three major classes of sphingolipids (Cers, Hex-Cers, and SMs) in respective strain/treatment combinations. P23H-P22, 22-day-old P23H-1 rhodopsin mutant rats; P23H-P45, 45-day-old P23H-1 rhodopsin mutant rats; SD-P22, 22-day-old Sprague-Dawley rats; SD-P45, 45-day-old Sprague-Dawley rats.

Hex-Cer were also higher in P23H-1 retina at P22 (**Table 2**; $P < 0.01$, $n = 4$). Treatment of FTY720 reduced the levels of most of these species such as C16:0, C20:0, C22:0, C24:1, C24:0, C26:1, and C26:0 (**Table 2**; $P < 0.01$, $n = 4$). Long-term FTY720 treatment appeared to affect the synthesis of Hex-Cers species in SD retinas but not in P23H-1 retinas at P45 (**Table 2**).

The relative compositional change in Hex-Cer also showed a similar pattern as found for Cer species; at P22, the relative mole % of shorter-chain species (16:0 + 18:0 + C20:0) of Hex-Cers reduced in P23H-1 retina, (54% to 46%), the relative composition of the longer-chain Hex-Cers (22:0, 24:1, and 24:0) were increased (46% to 54%) (supplementary Figure 2A vs. E), and FTY720 treatment reduced the difference in P23H-1 retina (supplementary Figure 2E vs. F).

From the Hex-Cer data at P45 (supplementary Figure 2C, D, G, H), it appears that P23H-1 retinas had higher levels of short-chain Cers and long-term treatment with FTY720 did not affect the ratio in both P23H-1 and SD retina.

Composition of SM species. Like Cer and Hex-Cers, most of the species of SM were increased in P23H-1 retina at P22 and at P45, and treatment of FTY720 had reduced the levels of some species of SM at P22 but not at P45 (**Table 3**; $P < 0.01$, $n = 4$). Very interestingly, the long-term treatment of FTY720 reduced the levels of the total as well as all major species of SM in SD retina (**Table 3**; $P < 0.01$, $n = 4$).

When we analyzed relative composition, at P22 we found downregulation of the shorter-chain SM species (C16:0 + C18:0), which is reduced from 63% to 56% in P23H-1 retina, and a similar increase in long-chain SM (C20:0 + C22:0 + C24:1 + C24:0) (37% to 44%), which is more similar to changes in its precursors Cers (supplementary Figure 3A vs. E). FTY720 treatment did not change the relative composition of SM in P22 SD retina; however, it slightly

reversed the ratio of both short-chain and long-chain SM in P23H-1 retina (supplementary Figure 3E vs. F).

From the SM data at P45 (supplementary Figure 3C, D, G, H), it appears that long-term treatment with FTY720 did not have much effect in the relative species distribution in both P23H-1 and SD retina.

In summary, we detected significant changes in the sphingolipid levels in the early stages of degeneration in P23H-1 retina. This is true for all three major classes of sphingolipids: Cers, Hex-Cers, and SM. By compositional analysis, we found a reduction in shorter-chain species of these lipids and an increase in longer-chain species in the P23H-1 retinas. Systemic FTY720 reduces the difference by increasing the shorter-chain species and decreasing the

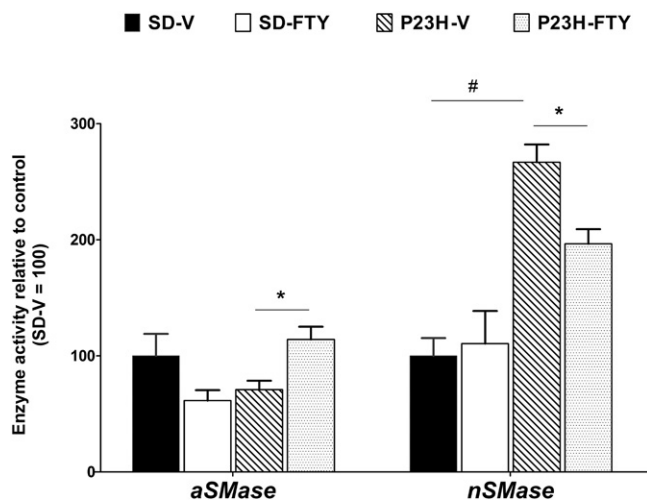


Fig. 5. Assay for acid and neutral SMases. Activity of aSMase and nSMase is represented in pmol of product formed/min/mg of protein relative to SD-V control. * $P < 0.05$ with respect to treatment with vehicle versus FTY720, # $P < 0.05$ with respect to strain differences in equivalent treatment conditions; Student's t -test ($n = 4$ samples/group).

TABLE 1. Composition of Cers from P23H-1 and SD retina at P22 and P45

Cer Species	P22				P45			
	SD-VH	SD-FTY	P23H-VH	P23H-FTY	SD-VH	SD-FTY	P23H-VH	P23H-FTY
C14:0	1.71 ± 0.24	1.53 ± 0.19	3.54 ± 0.71 ^a	3.25 ± 0.23	0.74 ± 0.15	0.59 ± 0.08	1.14 ± 0.04	1.32 ± 0.29
C16:0	82.08 ± 13.89	80.43 ± 11.06	119.76 ± 28.62	109.65 ± 7.51	55.42 ± 6.34	49.58 ± 5.96	40.56 ± 2.86	54.16 ± 12.25
C18:1	1.04 ± 0.12	0.91 ± 0.08	1.91 ± 0.53	1.67 ± 0.11	0.59 ± 0.06	0.45 ± 0.07	0.49 ± 0.04	0.63 ± 0.13
C18:0	128.52 ± 19.49	135.31 ± 21.32	218.51 ± 55.62	197.14 ± 16.19	119.10 ± 16.56	90.35 ± 16.08	92.41 ± 3.58	116.35 ± 25.84
C20:0	40.28 ± 6.06	37.18 ± 4.93	64.61 ± 12.74 ^a	53.69 ± 2.88	26.61 ± 1.60	26.12 ± 6.20	26.37 ± 2.24	30.57 ± 8.25
C22:0	10.83 ± 1.56	11.11 ± 2.05	22.72 ± 3.55 ^a	17.39 ± 0.90	7.07 ± 0.34	6.69 ± 1.48	8.13 ± 0.91	7.96 ± 1.64
C24:1	18.70 ± 2.14	17.65 ± 1.59	45.26 ± 6.29 ^a	37.93 ± 1.62	15.74 ± 2.26	12.60 ± 2.86	21.28 ± 3.09	20.29 ± 3.39
C24:0	7.96 ± 1.26	8.05 ± 1.55	21.67 ± 2.78 ^a	16.39 ± 1.19	5.70 ± 0.60	5.04 ± 1.04	6.41 ± 0.83	6.37 ± 1.41
C26:1	0.15 ± 0.01	0.15 ± 0.02	0.30 ± 0.04 ^a	0.24 ± 0.01	0.12 ± 0.0	0.07 ± 0.01	0.11 ± 0.01	0.11 ± 0.01
C26:0	0.01 ± 0.00	0.01 ± 0.00	0.02 ± 0.00 ^a	0.01 ± 0.00 ^b	0.12 ± 0.03	0.07 ± 0.00	0.06 ± 0.01	0.06 ± 0.01
Total	291.30 ± 44.54	292.33 ± 42.11	498.29 ± 106.04 ^a	437.37 ± 28.63	231 ± 22.70	191.56 ± 30.83	196.97 ± 12.13	237.83 ± 52.14

Rat pups are treated with FTY720 or vehicle (VH) starting at P10 and continued till harvest at P22 or P45. Absolute quantification (pmol/mg of tissue) values (mean ± SE) presented for each species.

^a Indicates significant change in P23H-1 retina from SD retina ($P < 0.01$, $n = 4$).

^b Indicates significant change after FTY720 treatment ($P < 0.01$, $n = 4$).

long-chain species. This particular effect of FTY720 on retinal sphingolipids was maintained to some extent in long-term treatment even in control SD rats.

Assessment of sphingolipid pathway genes

To identify the mechanism of FTY720 in the SD and P23H-1 rat retina, we investigated changes in gene expression and the activity of major Cer biosynthetic enzymes. In Fig. 6A, we show a simplified pathway of Cer biosynthesis in mammalian tissue. We performed detailed gene expression analysis of the Cer metabolic genes (Fig. 6B–D) by qRT-PCR. When we analyzed the expression of genes involved in de novo biosynthesis of Cer, such as *Spt1* (serine palmitoyl transferase 1), *Spt2*, *CerS2*, and *CerS4*, we found expression of both *Spt* were significantly higher in P23H-1 rats compared with SD rats, whereas *CerS4* had an opposite pattern (Fig. 6B; $P < 0.05$). In P23H-1 retinas, we observed a significant reduction in the expression of *Spt2*, *CerS2*, and *CerS4* after treatment with FTY720 compared with vehicle-treated controls (Fig. 6B; $P < 0.05$). We then analyzed expression of genes that encode enzymes for complex sphingolipid synthesis and degradation. We observed the expression of *Smpd1* (sphingomyelin phosphodiesterase 1) or aSMase in P23H-1 retinas was significantly reduced

when treated with FTY720 (Fig. 6C; $P < 0.05$). The expression of SM synthesis gene, *Sms1* (sphingomyelin synthase 1), was significantly higher in P23H-1 retina from SD retinas, which was downregulated by FTY720 treatment (Fig. 6C; $P < 0.05$). Similarly, expression of the glucosylceramide synthesis gene, *Gcs* (glucosylceramide synthase), or UDP-glucose ceramide glucosyltransferase and glucosylceramide hydrolyzing gene *Gba* (glucosidase β acid) were increased significantly in P23H-1 rats compared with those in SD rats (Fig. 6C; $P < 0.05$), and FTY720 treatment reduced the expression of *Gba* in P23H-1 (Fig. 6C; $P < 0.05$). We found no changes in the expression of major Cer degrading enzyme *Asah1* in P23H-1 rats, but the expression of *Sphks* (*sphk1*, *sphk2*) were significantly upregulated in P23H-1 retinas, which were reduced by FTY720 treatment (Fig. 6D; $P < 0.05$). We analyzed marker genes for apoptosis [Fos-like antigen 1 (*FosL1*)] and retinal stress (*Gfap1*) and, as expected, we found significant upregulation of their expression in P23H-1 retina (Fig. 6D; $P < 0.05$). We also verified few marker genes of inflammatory pathway such as *Il1b*, *Cxcl10*, *Il6*, *Ccl2*, and *Icam1* and found the relative expression of cytokine genes *Cxcl10* and *Ccl2* are significantly higher in P23H-1 retina compared with SD retinas; however, long-term

TABLE 2. Composition of Hex-Cers from P23H-1 and SD retina at P22 and P45

Hex-Cer Species	P22				P45			
	SD-VH	SD-FTY	P23H-VH	P23H-FTY	SD-VH	SD-FTY	P23H-VH	P23H-FTY
C14:0	0.06 ± 0.01	0.07 ± 0.01	0.10 ± 0.01	0.08 ± 0.01	0.27 ± 0.03	0.22 ± 0.02	0.37 ± 0.08	0.38 ± 0.07
C16:0	1.38 ± 0.13	1.11 ± 0.05	3.14 ± 0.24 ^a	2.37 ± 0.23 ^b	38.46 ± 1.4	31.69 ± 0.39 ^b	52.92 ± 2.16 ^a	54.56 ± 1.18
C18:1	0.11 ± 0.01	0.11 ± 0.01	0.16 ± 0.04 ^a	0.19 ± 0.03	0.25 ± 0.02	0.20 ± 0.02	0.31 ± 0.05	0.31 ± 0.05
C18:0	4.27 ± 0.53	3.50 ± 0.27	7.94 ± 1.53 ^a	6.13 ± 0.27	17.16 ± 0.64	14.15 ± 0.18 ^b	20.04 ± 0.29	19.39 ± 0.38
C20:0	2.87 ± 0.60	2.32 ± 0.46	6.30 ± 0.42 ^a	4.53 ± 0.43 ^b	10.45 ± 0.22	8.60 ± 0.34 ^b	12.91 ± 0.33	13.39 ± 0.23
C22:0	3.19 ± 0.77	2.47 ± 0.62	8.21 ± 0.73 ^a	4.83 ± 0.47 ^b	9.58 ± 0.38	7.26 ± 0.17 ^b	9.85 ± 0.35	9.46 ± 0.37
C24:1	0.88 ± 0.11	0.69 ± 0.14	2.85 ± 0.44 ^a	1.83 ± 0.19 ^b	17.94 ± 0.87	13.66 ± 0.47 ^b	17.45 ± 0.34	16.12 ± 0.15
C24:0	3.48 ± 0.65	2.65 ± 0.62	9.06 ± 0.79 ^a	6.08 ± 0.42 ^b	13.73 ± 1.47	9.79 ± 0.68 ^b	12.67 ± 0.16	11.47 ± 0.5
C26:1	0.02 ± 0.00	0.02 ± 0.01	0.06 ± 0.00 ^a	0.04 ± 0.00 ^b	0.72 ± 0.01	0.06 ± 0.00	0.10 ± 0.00	0.11 ± 0.00
C26:0	0.04 ± 0.01	0.03 ± 0.01	0.12 ± 0.01 ^a	0.07 ± 0.01 ^b	0.04 ± 0.00	0.04 ± 0.00	0.05 ± 0.00	0.05 ± 0.00
Total	16.30 ± 2.77	12.99 ± 1.86	37.94 ± 2.60 ^a	26.15 ± 1.67 ^b	107.95 ± 4.78	85.68 ± 1.35 ^b	126.67 ± 2.54	125.27 ± 1.95

Rat pups are treated with FTY720 or vehicle (VH) starting at P10 and continued till harvest at P22 or P45. Absolute quantification (pmol/mg of tissue) values (mean ± SE) presented for each species.

^a Indicates significant change in P23H-1 retina from SD retina ($P < 0.01$, $n = 4-6$).

^b Indicates significant change after FTY720 treatment ($P < 0.01$, $n = 4-6$).

TABLE 3. Composition of SM from P23H-1 and SD retina at P22 and P45

SM Species	P22				P45			
	SD-VH	SD-FTY	P23H-VH	P23H-FTY	SD-VH	SD-FTY	P23H-VH	P23H-FTY
C14:0	1.91 ± 0.09	2.05 ± 0.35	2.28 ± 0.11	2.18 ± 0.14	5.23 ± 1.13	3.38 ± 0.60	2.73 ± 0.76	2.88 ± 0.45
C16:0	53.49 ± 4.12	57.69 ± 2.91	79.39 ± 6.69 ^a	66.84 ± 3.78 ^b	270.26 ± 8.11	218.76 ± 9.69 ^b	136.08 ± 22.08 ^a	151.04 ± 16.47
C18:1	4.32 ± 0.32	4.35 ± 0.53	7.27 ± 0.54 ^a	5.20 ± 0.59	15.00 ± 1.33	9.55 ± 0.88 ^b	8.82 ± 1.60 ^a	8.86 ± 1.38
C18:0	59.44 ± 6.29	61.98 ± 4.01	87.31 ± 13.34 ^a	68.61 ± 4.37 ^b	290.00 ± 25.24	224.17 ± 7.92	182.13 ± 39.14 ^a	202.01 ± 20.33
C20:0	27.75 ± 2.02	29.45 ± 2.26	39.89 ± 2.65 ^a	31.05 ± 2.2	101.13 ± 7.76	78.81 ± 10.78	61.15 ± 10.70 ^a	64.08 ± 6.3
C22:0	13.35 ± 1.60	12.62 ± 1.53	25.45 ± 1.56 ^a	15.82 ± 1.16 ^b	45.60 ± 5.00	37.19 ± 10.77	30.05 ± 4.60	25.22 ± 5.92
C24:1	14.71 ± 1.18	13.66 ± 1.49	33.93 ± 2.97 ^a	17.48 ± 1.74 ^b	67.97 ± 1.07	41.13 ± 10.75 ^b	40.82 ± 5.03 ^a	38.08 ± 7.40
C24:0	12.02 ± 1.48	11.23 ± 1.70	27.13 ± 3.37 ^a	15.65 ± 1.81	33.68 ± 4.96	27.42 ± 3.39	25.49 ± 3.80 ^a	24.52 ± 7.02
C26:1	0.22 ± 0.02	0.19 ± 0.02	0.46 ± 0.05 ^a	0.26 ± 0.08 ^b	0.94 ± 0.22	0.45 ± 0.07 ^b	0.46 ± 0.07 ^a	0.49 ± 0.09
C26:0	0.32 ± 0.03	0.31 ± 0.02	0.62 ± 0.08 ^a	0.51 ± 0.07	0.54 ± 0.14	0.38 ± 0.06	0.30 ± 0.05 ^a	0.28 ± 0.08
Total	187.52 ± 16.78	193.55 ± 12.92	303.74 ± 15.69 ^a	223.60 ± 14.35 ^b	830.35 ± 23.17	641.24 ± 41.51 ^b	488.05 ± 6.05 ^a	518.37 ± 62.51

Rat pups are treated with FTY720 or vehicle (VH) starting at P10 and continued till harvest at P22 or P45. Absolute quantification (pmol/mg of tissue) values (mean ± SE) presented for each species.

^a Indicates significant change in P23H-1 retina from SD retina ($P < 0.01$, $n = 4$).

^b Indicates significant change after FTY720 treatment ($P < 0.01$, $n = 4$).

FTY720 did not block this increase (supplementary Figure 4; [#] $P < 0.05$).

In summary, the gene expression profile of sphingolipid metabolic genes largely correlated with sphingolipid profiles: the expression of the gene for an enzyme that increased in P23H-1 retina, correlated with the increase in metabolic product (lipid) of that particular enzyme, also increased, and the gene expression of which that had suppressed by FTY720 administration was well correlated with the decrease of their products.

IHC analysis of marker proteins

We analyzed the four groups of retinas from P35 rats for the photoreceptor markers, Müller cell and astrocyte markers, and S1P pathway proteins. SD and P23H-1 rat retinal sections in which the rhodopsin protein was detected after labeling with anti-rhodopsin antibodies (green) and cone outer segments were labeled with peanut agglutinin (Red). SD rats treated systemically with FTY720 seem to have no effect on rhodopsin and cone outer segment labeling and localization of these outer segment proteins (Fig. 7A, B). In P23H-1 retina rhodopsin mislocalization to the ONL was detected (Fig. 7C, D); however, the cone morphology appears to be normal. Serial retinal sections labeled with GS (green) and GFAP (red) in Fig. 7E–H. There was no change found in GS labeling in the P23H-1 retinas (Fig. 7G, H); however, GFAP expression and labeling markedly increased in P23H-1 retinas (Fig. 7G), and treatment of FTY720 reduced that expression (Fig. 7H). The serial sections were further labeled with SPHK2 (green) and ASAH1 (red) antibodies (Fig. 7I–L). No detectable changes in the labeling and localization of these sphingolipid metabolic marker proteins were detected in P23H-1 retinas and retinas from FTY720-treated rats. In summary, IHC studies indicated no adverse effect of FTY720 on the structure of major retinal cells in SD rats. Mislocalization of rhodopsin was apparent in P23H-1 retina but no change in cone opsin localization. Neuronal stress protein labeling was higher in P23H-1 retina, which appears to be decreased by FTY720 treatment.

DISCUSSION

Sphingolipids are a family of membrane lipids with important structural roles in the regulation of the fluidity and subdomain structure of the lipid bilayer, especially lipid rafts (32, 33); they also have crucial functional roles in receptor function, membrane conductance, cell-cell interactions, and the internalization of pathogens (16, 34). But their role in signaling has received wider attention in the last two decades since the discovery of Cer as a mediator of apoptotic cell death and S1P for cellular differentiation, migration, and protection from cell death (16, 17, 35, 36). It is now an established fact that bioactive sphingolipids, such as Cer, C1P, Sph, and S1P, maintain homeostasis at the cellular level as well as at tissue and system level by regulating cell growth, apoptosis, inflammation, fibrosis, angiogenesis, and so on (15, 16, 35, 37). The processes of apoptotic cell death is integral to major retinal diseases including RP, Stargardt's disease, Leber's congenital amaurosis, and AMD (38–41). Recent evidence suggests a strong correlation between Cer signaling and survival and homeostasis of photoreceptor and RPE cells (8, 42–48). In this study, we found significant alterations in the sphingolipid profile in P23H-1 rat retina at early age points (P22) when their photoreceptors begin to degenerate. Subsequently, early administration of the sphingolipid synthesizing and signaling modulator FTY720 was found to preserve the photoreceptors and delay the degeneration by restabilizing the sphingolipid profiles to some extent, thus supporting the fact that breakdown of the sphingolipid rheostat is associated with RD in this genetic rat model of human RDs. We previously determined that Cer levels increased in the rat model of light-induced RD before the start of active apoptosis, which could be reduced by systemic administration of FTY720 (8). Besides this, an increase in Cer levels has been shown in rd10 mice, which was associated with the progression of photoreceptor cell death. Inhibition of de novo Cer biosynthesis by myriocin in rd10 mice prevented the progress of retinal cell death (45). Further, involvement of Cer has been shown to be associated with a gradual loss of photoreceptor cells in an experimental model of retinal detachment in rabbits (38).

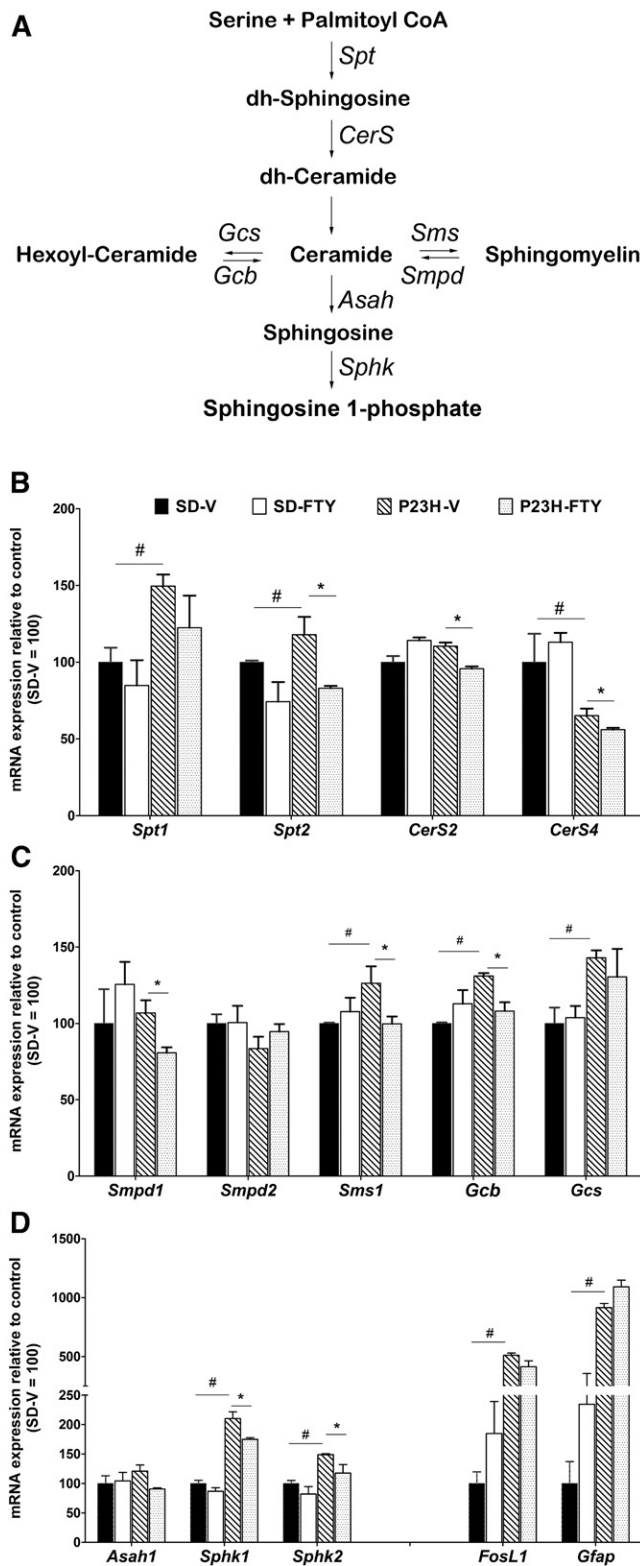


Fig. 6. Expression analysis of major sphingolipid metabolic genes. A: A representative flow chart of the major metabolic steps for generation of cellular Cers and conversion of Cers to other complex sphingolipids. The enzymes for each step were represented by the symbols of their respective genes. B: Expression of major enzymes involved in de novo Cer synthesis. Each sample included consisting of three independent qRT-PCR experiments that were averaged and normalized against two housekeeping genes; relative expression represented as \pm SE. Data represented relative to SD-V control, which is considered as 100. C: Expression of genes

There is more evidence of Cer's association of retinal cell death from in vitro cell culture studies and studies on *Drosophila* (42, 47, 49). This study with P23H-1 rats provides further evidence that alteration of Cer and other sphingolipid metabolites occurs during RD and their modulation by FTY720 can prevent degeneration. We therefore conclude that 1) upregulation of Cer and its metabolites in the degenerating retina may be a common event secondary to stress or genetic mutation leading to RD; 2) these metabolites can serve as second messengers involved in photoreceptor cell death; 3) inhibiting these second messengers could have therapeutic benefits, and 4) U.S. Food and Drug Administration (FDA)-approved drug FTY720 or its derivatives could be developed as novel therapeutics for RD diseases, as this can modulate the sphingolipid profile of the damaged or diseased retina by systemic administration.

P23H rats are a commonly used model for studying the dominant form of RD because they carry the most frequent mutation in adRP in the United States (41). P23H rats express rhodopsin transgene with a single amino acid substitution at codon 23, which leads to rhodopsin misfolding, endoplasmic reticulum stress, and activation of the unfolded protein response, which eventually leads to rod photoreceptor degeneration (50, 51). This is the first report of sphingolipid profile in P23H-1 retina. Unlike our previous study on light-induced retinal degeneration samples where only the Cers and lyso-phosphatidic species of Sphs were analyzed, here we included the Hex-Cer species and SM. SMs are the major class of sphingolipids in most tissues including the neural tissues, which are present in the membrane. In adult retina, they comprise >70% of the total nonsialylated sphingolipids (52). The P45 retina from SD rats confirms this composition; however, the ratio of SM to simpler Cers (Cer and Hex-Cers) is reduced in P23H-1 retina (Fig. 4). We found the composition of major sphingolipids in P22 retina is very different with higher percentage of Cer and Hex-Cer compared with P45 in both SD and P23H-1 rats (Fig. 4).

Absolute quantification, however, indicated the accumulation of sphingolipid metabolites, Cer, the key component of all sphingolipids, and more profoundly the metabolites that are generated from Cers such as Hex-Cer, SM, and S1P in P22 P23H-1 retina. Numerous pieces of evidence indicate that Cer, the core lipid of sphingolipid metabolism, is a key factor in apoptotic cell death (16). Various external stressors, such as chemotherapeutic agents, heat, UV radiation, and lipopolysaccharides have been shown to increase intracellular Cer levels and signal for cell death (53). Accumulation of Cer itself but more of its products in P23H-1 retina might indicate an upregulation

involved in complex sphingolipid synthesis from Cer and breakdown. D: Expression of downstream Cer catabolic genes and stress response enzymes. *FosL1*, Fos-like antigen 1; *Gcb*, glucosidase β . * $P < 0.05$ with respect to vehicle treatment versus FTY; # $P < 0.05$ with respect to strain differences in equivalent treatment conditions; Student's *t*-test ($n = 4$ samples/group).

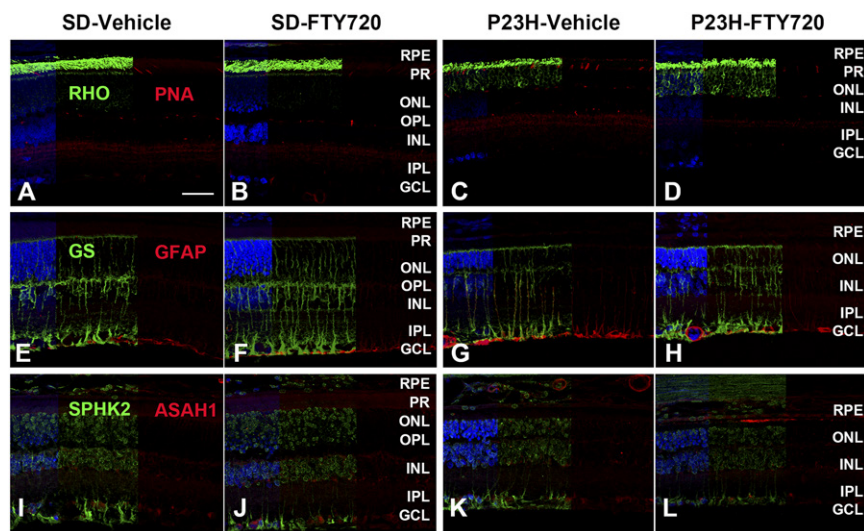


Fig. 7. IHC analysis of rat retina for photoreceptor markers, Müller cell and astrocyte markers, and S1P pathway markers. A–D: Rhodopsin (RHO, green) and peanut agglutinin (PNA, red). A: SD rat retinal section in which the rhodopsin protein was detected after labeling with anti-rhodopsin antibodies (green) and cone outer segments were labeled with PNA (Red). B: SD rats treated systemically with FTY720. C: P23H-1, vehicle-treated retinas. D: P23H1 FTY720-treated retinas. E–H: Same series of retinal sections labeled with GS (green) and GFAP (red). I–L: Same series of retinal sections labeled with SPHK2 (green) and ASAH1 (red).

of the genes for enzymes that use Cer as a substrate, which could be a cellular survival response to maintain the non-toxic level of Cer. FTY720 is known to inhibit Cer synthase and block Cer synthesis in the *de novo* pathway, but it is not known for any action on the enzymes in the Cer-catabolic pathway. The reducing trend found in Hex-Cer, SM, and S1P upon FTY720 treatment might also suggest the above hypothesis that FTY720 inhibited Cer synthesis, which eventually reduced Cer metabolic products. However, no change in Cer level upon FTY720 treatment indicates there may be other pathways of Cer generation being activated such as the SMase pathway (Fig. 6A). We indeed observed increase in nSMase activity P23H-1 retina; FTY720 treatment could reduce this activity to some extent (albeit not to the normal level), but at the same time increased aSMase activity, which maintained the higher levels of Cer in P23H-1 retina (Fig. 5). Hex-Cer and SM are more important as membrane components but less connected with biological activity, unlike Cer and S1P, which are highly bioactive. There is evidence that S1P can reduce Cer generation by inhibiting Cer synthase in a feedback mechanism (54). Thus, the changes in the major sphingolipids in P23H-1 retina indicate a cellular response associated with the dysregulation of sphingolipids, which could be acting as secondary metabolites in the process of retinal cell death. The rebalance of this change of sphingolipids by FTY720 thus explains how this could prevent cell death and delay the degeneration of P23H-1 retina.


There could be hundreds of sphingolipid species in a cell depending on the fatty acid chain length, presence and number of double bonds, and the modification in the head group (31). When we investigated the composition of major Cer, Hex-Cer, and SM species, we found a

significant increase in the long-chain species and decrease in shorter-chain species in P23H-1 retina. Treatment with FTY720 could rebalance the ratio by reducing the long-chain and increasing the short-chain species (supplementary Figures 1–3). Cellular Cers are synthesized by CerSs, and the chain length depends on the activity of specific CerSs. So far, six different mammalian CerSs (CerS1–6) have been described. CerS1 synthesizes mainly C18-Cer, CerS4 synthesizes C18-/C20-/C24-Cer, CerS5 and CerS6 synthesize mostly C14-/C16-/C18-Cer, CerS2 synthesizes preferentially C22-/C24-Cer, and CerS3 synthesizes very long chain Cers (>C26-Cer) (55–58). CerS1 and CerS4 have higher expression in neural tissue (56), and our expression studies in rat and mouse retina confirm relatively higher expression of CerS1, CerS2, and CerS4 in the retina (data not shown). CerS1 and CerS4 are specific to synthesis of Cers with chain length C18–20 and CerS2 for C20–26. Numerous cell culture studies suggest that short-chain Cers, especially, C16, are proapoptotic, and long chains such as C22:0, C24:0, and C24:1 are antiapoptotic or pro-proliferative (59–62). Increases in long-chain species in P23H-1 retina could therefore be a cellular response to counter the apoptosis of photoreceptor cells that is induced by genetic mutation, ER stress, and activation of the unfolded protein response. Cer signaling, however, is very complex, the intricacies within the roles of various chain-length Cers, Hex-Cers, and SM are not known. It has been reported that in brain tissue samples from Alzheimer's disease (AD) patients, the abundance of C18:0 and C24:0 Cers increase with disease severity, whereas the levels of C16, C20, and C22 Cers remain unchanged (63). This may indicate, in AD patients, either the activity or the expression levels of CerS1 and CerS2 increase with disease severity. In vitro data demonstrate that, in cultured hippocampal

neurons exposed to amyloid β 1-42, the levels of C18:0 and C24:0 Cer increased. These could be inhibited by blocking Cer production using myriocin (an inhibitor of Spt, the rate-limiting step in de novo sphingolipid synthesis) (63). In cultured osteoblasts, the induction of apoptosis by sodium nitroprusside causes C22:0, C24:0, and/or C24:1 Cer levels to increase, whereas other Cer species are unaffected (64). To clarify the impact of other Cers in ionizing radiation (IR)-induced apoptosis, Mesicek et al. (65) determined the levels of Cers in HeLa cells after IR treatment and found increased levels of C16:0, C24:0, and C24:1 Cers, probably due to enhanced CerS activity, because these effects could be blocked by the CerS inhibitor fumonisin B1. These data suggest an association of long-chain Cers with apoptosis; however, the specific roles of these in the process of cell death are yet to be identified.

Cers are synthesized mainly by two pathways: the de novo pathway and the breakdown from complex sphingolipids, SM, and glycosyl ceramides. As evidenced in the past and our studies in the retina, the Cer species that are induced to cause apoptosis are produced through the de novo pathway (8, 56). FTY720 is a de novo Cer synthesis inhibitor; FTY720 can inhibit all of the six CerS isozymes with CerS4 being the least inhibited (9, 10, 23). In vitro kinetic studies suggest that FTY720 is a potent and competitive inhibitor of CerS2 compared with classical CerS inhibitor fumonisin B1 to inhibit the de novo biosynthesis of 24:1 and 24:0 CerS (9). Our in vivo studies in rats correlate with this notion; systemic FTY720 reduced the levels of C24:0 and C24:1 in both P23H-1 and SD rat retina (supplementary Figures 1–3 and Tables 1–3) most probably by inhibiting CerS2 activity.

Gene expression analysis correlated with the sphingolipid profiles of the P23H-1 retina and the effect of FTY720 (Fig. 6). Expression of the very first enzymes for de novo Cer biosynthesis (*Spt1*, *Spt2*) were significantly higher in the P23H-1 retina; however, a reduction of the mRNA of the enzymes in the immediate following step (*CerS2*, *CerS4*) may be associated to reduce the flux of de novo Cer. Increase in *Sms1* and *Gcs* might have caused the increase in SM and Hex-Cer and the reduction in *Smpds*, thus preventing the breakdown of the accumulated SM (Fig. 6). Similarly, significant increases in the expression of *Sphks* might be associated with the increase in the levels of SIP. FTY720 treatment reduced the expression of most of the genes that are associated with the increase in the levels of enzymes involved in Cer and SIP generation that are known to be potent signaling sphingolipids, such as *Spt2*, *CerS2*, *CerS4*, *Smpd1*, *Gcb*, and *Sphks* (Fig. 6). We found a significant increase in nSMase activity (SMPD2) in P23H-1 retina; however, mRNA expression was not changed (Figs. 5, 6), which we predict might have contributed in the increased Cer in the retina. Neutral SMase is one of the key enzymes involved in the generation of Cer, which is more specific to neural cells and can be activated by diverse molecules like TNF α , oxidized human LDLs, and several growth factors (66). Thus, it is apparent that alteration of the sphingolipid profile in P23H-1 rat retina resulted from significant changes in gene expression as well as the activity

of major enzymes, and we believe FTY720 interfered in both the gene expression level and enzyme activity. FTY720-mediated neuroprotection is documented well in many recent publications including our previous publication (8, 67–71). The minute details of how FTY720 influenced retinal gene expression and enzyme activity for sphingolipid biosynthesis needs to be demonstrated in future studies. It must be noted that during clinical trials for multiple sclerosis high dose of FTY720 caused macular edema in some patients, which is usually a manifestation of nonspecific inflammation in the retina (11). However, further studies using high resolution SD-OCT has led to the finding of a 4.7% incidence of microcystic macular edema in patients with multiple sclerosis, none of whom were on FTY720 therapy (72). We believe that modulation of retinal sphingolipids in healthy eyes may cause inflammation, the mechanism of which is not very clear. However, in disease states where there is a dysregulation of sphingolipids, FTY720 can effectively rebalance the level. Therefore, from the therapeutic development point of view, the potential for FTY720 use in RD could still be very high. Because of the highly heterogeneous nature of the disease, there is a lack of specific targets for developing preventative and curative therapies for RDs. Increases in Cer and its metabolites being a secondary event could be common in more than one form of RD that occurs from mutations in many diverse genes. Our data clearly indicate that FTY720 can modulate the sphingolipid metabolism in the retina and thus provide a potential therapeutic option to explore and develop for retinal degenerative diseases using this FDA-approved drug and related compounds. 

REFERENCES

1. Adamis, A. P., and A. J. Berman. 2008. Immunological mechanisms in the pathogenesis of diabetic retinopathy. *Semin. Immunopathol.* **30**: 65–84.
2. Chen, H., A. Y. Chan, D. U. Stone, and N. A. Mandal. 2014. Beyond the cherry-red spot: Ocular manifestations of sphingolipid-mediated neurodegenerative and inflammatory disorders. *Surv. Ophthalmol.* **59**: 64–76.
3. Chen, L., W. Wu, T. Dentchev, Y. Zeng, J. Wang, I. Tsui, J. W. Tobias, J. Bennett, D. Baldwin, and J. L. Dunaief. 2004. Light damage induced changes in mouse retinal gene expression. *Exp. Eye Res.* **79**: 239–247.
4. Donoso, L. A., D. Kim, A. Frost, A. Callahan, and G. Hageman. 2006. The role of inflammation in the pathogenesis of age-related macular degeneration. *Surv. Ophthalmol.* **51**: 137–152.
5. Hollyfield, J. G., V. L. Bonilha, M. E. Rayborn, X. Yang, K. G. Shadrach, L. Lu, R. L. Ufret, R. G. Salomon, and V. L. Perez. 2008. Oxidative damage-induced inflammation initiates age-related macular degeneration. *Nat. Med.* **14**: 194–198.
6. Kern, T. S. 2007. Contributions of inflammatory processes to the development of the early stages of diabetic retinopathy. *Exp. Diabetes Res.* **2007**: 95103.
7. Zhou, J., Y. P. Jang, S. R. Kim, and J. R. Sparrow. 2006. Complement activation by photooxidation products of A2E, a lipofuscin constituent of the retinal pigment epithelium. *Proc. Natl. Acad. Sci. USA.* **103**: 16182–16187.
8. Chen, H., J. T. Tran, A. Eckerd, T. P. Huynh, M. H. Elliott, R. S. Brush, and N. A. Mandal. 2013. Inhibition of de novo ceramide biosynthesis by FTY720 protects rat retina from light-induced degeneration. *J. Lipid Res.* **54**: 1616–1629.
9. Berdyshev, E. V., I. Gorshkova, A. Skobeleva, R. Bittman, X. Lu, S. M. Dudek, T. Mirzapoiazova, J. G. Garcia, and V. Natarajan.

2009. FTY720 inhibits ceramide synthases and up-regulates dihydrosphingosine 1-phosphate formation in human lung endothelial cells. *J. Biol. Chem.* **284**: 5467–5477.
10. Lahiri, S., H. Park, E. L. Laviad, X. Lu, R. Bittman, and A. H. Futerman. 2009. Ceramide synthesis is modulated by the sphingosine analog FTY720 via a mixture of uncompetitive and noncompetitive inhibition in an Acyl-CoA chain length-dependent manner. *J. Biol. Chem.* **284**: 16090–16098.
 11. Cohen, J. A., F. Barkhof, G. Comi, H. P. Hartung, B. O. Khatri, X. Montalban, J. Pelletier, R. Capra, P. Gallo, G. Izquierdo, et al. 2010. Oral fingolimod or intramuscular interferon for relapsing multiple sclerosis. *N. Engl. J. Med.* **362**: 402–415.
 12. Edmonds, Y., S. Milstien, and S. Spiegel. 2011. Development of small-molecule inhibitors of sphingosine-1-phosphate signaling. *Pharmacol. Ther.* **132**: 352–360.
 13. Suzuki, S., S. Enosawa, T. Kakefuda, T. Shinomiya, M. Amari, S. Naoe, Y. Hoshino, and K. Chiba. 1996. A novel immunosuppressant, FTY720, with a unique mechanism of action, induces long-term graft acceptance in rat and dog allotransplantation. *Transplantation.* **61**: 200–205.
 14. Zemann, B., B. Kinzel, M. Muller, R. Reuschel, D. Mechtcheriakova, N. Urtz, F. Bornancin, T. Baumruker, and A. Billich. 2006. Sphingosine kinase type 2 is essential for lymphopenia induced by the immunomodulatory drug FTY720. *Blood.* **107**: 1454–1458.
 15. Futerman, A. H., and Y. A. Hannun. 2004. The complex life of simple sphingolipids. *EMBO Rep.* **5**: 777–782.
 16. Hannun, Y. A., and L. M. Obeid. 2008. Principles of bioactive lipid signalling: lessons from sphingolipids. *Nat. Rev. Mol. Cell Biol.* **9**: 139–150.
 17. Obeid, L. M., C. M. Linardic, L. A. Karolak, and Y. A. Hannun. 1993. Programmed cell death induced by ceramide. *Science.* **259**: 1769–1771.
 18. Pettus, B. J., C. E. Chalfant, and Y. A. Hannun. 2004. Sphingolipids in inflammation: roles and implications. *Curr. Mol. Med.* **4**: 405–418.
 19. Zhang, H., N. N. Desai, A. Olivera, T. Seki, G. Brooker, and S. Spiegel. 1991. Sphingosine-1-phosphate, a novel lipid, involved in cellular proliferation. *J. Cell Biol.* **114**: 155–167.
 20. Aktas, O., P. Kury, B. Kieseier, and H. P. Hartung. 2010. Fingolimod is a potential novel therapy for multiple sclerosis. *Nat. Rev. Neurol.* **6**: 373–382.
 21. Kappos, L., E. W. Radue, P. O'Connor, C. Polman, R. Hohlfeld, P. Calabresi, K. Selmaj, C. Agoropoulou, M. Leyk, L. Zhang-Auberson, et al. 2010. A placebo-controlled trial of oral fingolimod in relapsing multiple sclerosis. *N. Engl. J. Med.* **362**: 387–401.
 22. Massberg, S., and U. H. von Andrian. 2006. Fingolimod and sphingosine-1-phosphate—modifiers of lymphocyte migration. *N. Engl. J. Med.* **355**: 1088–1091.
 23. Schiffmann, S., D. Hartmann, S. Fuchs, K. Birod, N. Ferreiros, Y. Schreiber, A. Zivkovic, G. Geisslinger, S. Grosch, and H. Stark. 2012. Inhibitors of specific ceramide synthases. *Biochimie.* **94**: 558–565.
 24. Machida, S., M. Kondo, J. A. Jamison, N. W. Khan, L. T. Kononen, T. Sugawara, R. A. Bush, and P. A. Sieving. 2000. P23H rhodopsin transgenic rat: correlation of retinal function with histopathology. *Invest. Ophthalmol. Vis. Sci.* **41**: 3200–3209.
 25. Pennesi, M. E., S. Nishikawa, M. T. Matthes, D. Yasumura, and M. M. LaVail. 2008. The relationship of photoreceptor degeneration to retinal vascular development and loss in mutant rhodopsin transgenic and RCS rats. *Exp. Eye Res.* **87**: 561–570.
 26. Wijesinghe, D. S., J. C. Allegood, L. B. Gentile, T. E. Fox, M. Kester, and C. E. Chalfant. 2010. Use of high performance liquid chromatography-electrospray ionization-tandem mass spectrometry for the analysis of ceramide-1-phosphate levels. *J. Lipid Res.* **51**: 641–651.
 27. Wijesinghe, D. S., M. Brentnall, J. A. Mietla, L. A. Hoeflerlin, R. F. Diegelmann, L. H. Boise, and C. E. Chalfant. 2014. Ceramide kinase is required for a normal eicosanoid response and the subsequent orderly migration of fibroblasts. *J. Lipid Res.* **55**: 1298–1309.
 28. Mandal, M. N., R. Ambasudhan, P. W. Wong, P. J. Gage, P. A. Sieving, and R. Ayyagari. 2004. Characterization of mouse orthologue of ELOVL4: genomic organization and spatial and temporal expression. *Genomics.* **83**: 626–635.
 29. Mandal, M. N., and R. Ayyagari. 2006. Complement factor H: spatial and temporal expression and localization in the eye. *Invest. Ophthalmol. Vis. Sci.* **47**: 4091–4097.
 30. Mandal, N. A., J. T. Tran, A. Saadi, A. K. Rahman, T. P. Huynh, W. H. Klein, and J. H. Cho. 2013. Expression and localization of CERKL in the mammalian retina, its response to light-stress, and relationship with NeuroD1 gene. *Exp. Eye Res.* **106**: 24–33.
 31. Hannun, Y. A., and L. M. Obeid. 2011. Many ceramides. *J. Biol. Chem.* **286**: 27855–27862.
 32. Martin, R. E., M. H. Elliott, R. S. Brush, and R. E. Anderson. 2005. Detailed characterization of the lipid composition of detergent-resistant membranes from photoreceptor rod outer segment membranes. *Invest. Ophthalmol. Vis. Sci.* **46**: 1147–1154.
 33. Tsui-Pierchala, B. A., M. Encinas, J. Milbrandt, and E. M. Johnson, Jr. 2002. Lipid rafts in neuronal signaling and function. *Trends Neurosci.* **25**: 412–417.
 34. Huwiler, A., T. Kolter, J. Pfeilschifter, and K. Sandhoff. 2000. Physiology and pathophysiology of sphingolipid metabolism and signaling. *Biochim. Biophys. Acta.* **1485**: 63–99.
 35. Olivera, A., and S. Spiegel. 1993. Sphingosine-1-phosphate as second messenger in cell proliferation induced by PDGF and FCS mitogens. *Nature.* **365**: 557–560.
 36. Maceyka, M., and S. Spiegel. 2014. Sphingolipid metabolites in inflammatory disease. *Nature.* **510**: 58–67.
 37. Spiegel, S., and S. Milstien. 2003. Sphingosine-1-phosphate: an enigmatic signalling lipid. *Nat. Rev. Mol. Cell Biol.* **4**: 397–407.
 38. Allikmets, R. 2004. Leber congenital amaurosis: a genetic paradigm. *Ophthalmic Genet.* **25**: 67–79.
 39. Glazer, L. C., and T. P. Dryja. 2003. Understanding the etiology of Stargardt's disease. *Ophthalmol. Clin. North Am.* **15**: 93–100.
 40. Haddad, S., C. A. Chen, S. L. Santangelo, and J. M. Seddon. 2006. The genetics of age-related macular degeneration: a review of progress to date. *Surv. Ophthalmol.* **51**: 316–363.
 41. Hartong, D. T., E. L. Berson, and T. P. Dryja. 2006. Retinitis pigmentosa. *Lancet.* **368**: 1795–1809.
 42. German, O. L., G. E. Miranda, C. E. Abrahan, and N. P. Rotstein. 2006. Ceramide is a mediator of apoptosis in retina photoreceptors. *Invest. Ophthalmol. Vis. Sci.* **47**: 1658–1668.
 43. Rotstein, N. P., G. E. Miranda, C. E. Abrahan, and O. L. German. 2010. Regulating survival and development in the retina: key roles for simple sphingolipids. *J. Lipid Res.* **51**: 1247–1262.
 44. Ranty, M. L., S. Carpentier, M. Cournot, I. Rico-Lattes, F. Malecaze, T. Levade, M. B. Delisle, and J. C. Quintyn. 2009. Ceramide production associated with retinal apoptosis after retinal detachment. *Graefes Arch. Clin. Exp. Ophthalmol.* **247**: 215–224.
 45. Strettoi, E., C. Gargini, E. Novelli, G. Sala, I. Piano, P. Gasco, and R. Ghidoni. 2010. Inhibition of ceramide biosynthesis preserves photoreceptor structure and function in a mouse model of retinitis pigmentosa. *Proc. Natl. Acad. Sci. USA.* **107**: 18706–18711.
 46. Chen, H., J. T. Tran, R. S. Brush, A. Saadi, A. K. Rahman, M. Yu, D. Yasumura, M. T. Matthes, K. Ahern, H. Yang, et al. 2012. Ceramide signaling in retinal degeneration. *Adv. Exp. Med. Biol.* **723**: 553–558.
 47. Acharya, U., S. Patel, E. Koundakjian, K. Nagashima, X. Han, and J. K. Acharya. 2003. Modulating sphingolipid biosynthetic pathway rescues photoreceptor degeneration. *Science.* **299**: 1740–1743.
 48. Zhu, D., P. G. Sreekumar, D. R. Hinton, and R. Kannan. 2010. Expression and regulation of enzymes in the ceramide metabolic pathway in human retinal pigment epithelial cells and their relevance to retinal degeneration. *Vision Res.* **50**: 643–651.
 49. Sanvicens, N., and T. G. Cotter. 2006. Ceramide is the key mediator of oxidative stress-induced apoptosis in retinal photoreceptor cells. *J. Neurochem.* **98**: 1432–1444.
 50. Sung, C. H., C. M. Davenport, J. C. Hennessey, I. H. Maumenee, S. G. Jacobson, J. R. Heckenlively, R. Nowakowski, G. Fishman, P. Gouras, and J. Nathans. 1991. Rhodopsin mutations in autosomal dominant retinitis pigmentosa. *Proc. Natl. Acad. Sci. USA.* **88**: 6481–6485.
 51. Sung, C. H., C. M. Davenport, and J. Nathans. 1993. Rhodopsin mutations responsible for autosomal dominant retinitis pigmentosa. Clustering of functional classes along the polypeptide chain. *J. Biol. Chem.* **268**: 26645–26649.
 52. Brush, R. S., J. T. Tran, K. R. Henry, M. E. McClellan, M. H. Elliott, and M. N. Mandal. 2010. Retinal sphingolipids and their very-long-chain fatty acid-containing species. *Invest. Ophthalmol. Vis. Sci.* **51**: 4422–4431.
 53. Nikolova-Karakashian, M. N., and K. A. Rozenova. 2010. Ceramide in stress response. *Adv. Exp. Med. Biol.* **688**: 86–108.
 54. Laviad, E. L., L. Albee, I. Pankova-Kholmiansky, S. Epstein, H. Park, A. H. Merrill, Jr., and A. H. Futerman. 2008. Characterization of ceramide synthase 2: tissue distribution, substrate specificity, and inhibition by sphingosine 1-phosphate. *J. Biol. Chem.* **283**: 5677–5684.

55. Mullen, T. D., Y. A. Hannun, and L. M. Obeid. 2012. Ceramide synthases at the centre of sphingolipid metabolism and biology. *Biochem. J.* **441**: 789–802.
56. Grösch, S., S. Schiffmann, and G. Geisslinger. 2012. Chain length-specific properties of ceramides. *Prog. Lipid Res.* **51**: 50–62.
57. Stüban, J., R. Tidhar, and A. H. Futerman. 2010. Ceramide synthases: roles in cell physiology and signaling. *Adv. Exp. Med. Biol.* **688**: 60–71.
58. Levy, M., and A. H. Futerman. 2010. Mammalian ceramide synthases. *IUBMB Life.* **62**: 347–356.
59. Hartmann, D., J. Lucks, S. Fuchs, S. Schiffmann, Y. Schreiber, N. Ferreiros, J. Merckens, R. Marschalek, G. Geisslinger, and S. Grosch. 2012. Long chain ceramides and very long chain ceramides have opposite effects on human breast and colon cancer cell growth. *Int. J. Biochem. Cell Biol.* **44**: 620–628.
60. Thomas, R. L., Jr., C. M. Matsko, M. T. Lotze, and A. A. Amoscato. 1999. Mass spectrometric identification of increased C16 ceramide levels during apoptosis. *J. Biol. Chem.* **274**: 30580–30588.
61. Osawa, Y., H. Uchinami, J. Bielawski, R. F. Schwabe, Y. A. Hannun, and D. A. Brenner. 2005. Roles for C16-ceramide and sphingosine 1-phosphate in regulating hepatocyte apoptosis in response to tumor necrosis factor- α . *J. Biol. Chem.* **280**: 27879–27887.
62. Seumois, G., M. Fillet, L. Gillet, C. Faccinotto, C. Desmet, C. Francois, B. Dewals, C. Oury, A. Vanderplasschen, P. Lekeux, et al. 2007. De novo C16- and C24-ceramide generation contributes to spontaneous neutrophil apoptosis. *J. Leukoc. Biol.* **81**: 1477–1486.
63. Cutler, R. G., J. Kelly, K. Storie, W. A. Pedersen, A. Tammara, K. Hatanpaa, J. C. Troncoso, and M. P. Mattson. 2004. Involvement of oxidative stress-induced abnormalities in ceramide and cholesterol metabolism in brain aging and Alzheimer's disease. *Proc. Natl. Acad. Sci. USA.* **101**: 2070–2075.
64. Olivier, S., M. Fillet, M. Malaise, J. Piette, V. Bours, M. P. Merville, and N. Franchimont. 2005. Sodium nitroprusside-induced osteoblast apoptosis is mediated by long chain ceramide and is decreased by raloxifene. *Biochem. Pharmacol.* **69**: 891–901.
65. Mesicek, J., H. Lee, T. Feldman, X. Jiang, A. Skobeleva, E. V. Berdyshev, A. Haimovitz-Friedman, Z. Fuks, and R. Kolesnick. 2010. Ceramide synthases 2, 5, and 6 confer distinct roles in radiation-induced apoptosis in HeLa cells. *Cell. Signal.* **22**: 1300–1307.
66. Chatterjee, S. 1999. Neutral sphingomyelinase: past, present and future. *Chem. Phys. Lipids.* **102**: 79–96.
67. Slowik, A., T. Schmidt, C. Beyer, S. Amor, T. Clarner, and M. Kipp. 2015. The sphingosine 1-phosphate receptor agonist FTY720 is neuroprotective after cuprizone-induced CNS demyelination. *Br. J. Pharmacol.* **172**: 80–92.
68. Rolland II, W. B., A. Manaenko, T. Lekic, Y. Hasegawa, R. Ostrowski, J. Tang, and J. H. Zhang. 2011. FTY720 is neuroprotective and improves functional outcomes after intracerebral hemorrhage in mice. *Acta Neurochir. Suppl.* **111 (Suppl.)**: 213–217.
69. Noda, H., H. Takeuchi, T. Mizuno, and A. Suzumura. 2013. Fingolimod phosphate promotes the neuroprotective effects of microglia. *J. Neuroimmunol.* **256**: 13–18.
70. Liesz, A., L. Sun, W. Zhou, S. Schwarting, E. Mracsco, M. Zorn, H. Bauer, C. Sommer, and R. Veltkamp. 2011. FTY720 reduces post-ischemic brain lymphocyte influx but does not improve outcome in permanent murine cerebral ischemia. *PLoS One.* **6**: e21312.
71. Di Menna, L., G. Molinaro, L. Di Nuzzo, B. Riozzi, C. Zappulla, C. Pozzilli, R. Turrini, F. Caraci, A. Copani, G. Battaglia, et al. 2013. Fingolimod protects cultured cortical neurons against excitotoxic death. *Pharmacol. Res.* **67**: 1–9.
72. Gelfand, J. M., R. Nolan, D. M. Schwartz, J. Graves, and A. J. Green. 2012. Microcystic macular oedema in multiple sclerosis is associated with disease severity. *Brain.* **135**: 1786–1793.